Original Article

Institution of MECHANICAL ENGINEERS

Journal of MECHANICAL ENGINEERING SCIENCE

Proc IMechE Part C:
J Mechanical Engineering Science
0(0) 1–15

DOI: 10.1177/0954406220930049
journals.sagepub.com/home/pic
SAGE

Investigations on friction stir joining of 3D printed parts to overcome bed size limitation and enhance joint quality for unmanned aircraft systems

Vivek Kumar Tiwary, N J Ravi, P Arunkumar, S Shivakumar, Anand S Deshpande and Vinayak R Malik

Abstract

3D printing technology is making its mark in automotive, aerospace, and bio-medical-related industries. It is considered a viable option for the direct manufacturing of final parts. However, it is not possible to print longer parts in a single attempt due to the bed size limitation of printers. This problem can be addressed by employing a polymer joining technique as a secondary operation. Moreover, low mechanical strength and inferior geometrical qualities like the flatness of the joined parts restrict its real-time industrial application. Here, an attempt is made to join a longer part (typical of an aircraft wing) using friction stir welding technique. Joining was performed on 3D printed similar/dissimilar thermoplastic parts. Tensile test results showed that friction stir welding of 3D printed parts (for both similar/dissimilar) produced relatively weaker joints compared to the base material. Various important process parameters of 3D printing and friction stir welding technique, namely part infill percentage, material combination, tool rotational speed, traverse speed, and tool pin taper angle were optimized by means of ANOVA. Optimization was aimed at maximizing the weld strength, elongation, hardness, and desired flatness. The results suggested that the material combination and tool pin taper angle play a significant role in the weld's strength as well as its geometric properties (flatness). The results were validated by adopting the optimized parameters for successful joining of the wing section of an unmanned aerial vehicle. A span of 320 mm, with a metrological acceptable flatness value of 0.41 μ/m could be successfully achieved on an existing 3D printer whose bed size limit was 240 mm.

Keywords

3D printing, fused deposition modeling, friction stir welding of polymers, flatness, unmanned aerial vehicle, printing volume limitation

Date received: 5 December 2019; accepted: 4 May 2020

Introduction

Additive manufacturing (AM) also popularly known as rapid prototyping (RP) or 3D printing (3DP) is a very exciting technology that quickly converts a scaled CAD model into an actual physical object by layer-to-layer addition of materials. Among the various technologies available in market, fused deposition modeling (FDM) is one of the most accepted technique. Ability to produce complex parts, larger design flexibility, low weight with improved performance, low cost, minimal material wastage, and decreased product development time makes this one of the trendiest manufacturing technology.[1–3] The first step in 3DP-FDM printing is generation of a .STL file using CAD software. The CAD model is then sliced into layers wherein the infill percentages, thickness of each layer, raster angle, and other parameters are set. When the 3D printing process is performed on the machine, a thermo-plastic polymeric filament oozes out through a heated nozzle onto a print platform (bed). The required force for the extrusion of the polymeric filaments is created using a gear

Department of Mechanical Engineering, KLS Gogte Institute of Technology, Belagavi, India

Corresponding authors:
Vivek Kumar Tiwary, Department of Mechanical Engineering, KLS Gogte Institute of Technology, Belagavi 590008, Karnataka, India.
Email: vgtiwary@git.edu

Vinayak R Malik, Department of Mechanical Engineering, KLS Gogte Institute of Technology, Belagavi 590008, Karnataka, India.
Emails: vrm@git.edu, vinayakmalik008@gmail.com

and bearing mechanism. Based on the component's cross-section, the controller software controls the movement of the nozzle over the bed. After one layer is printed, either the nozzle or the bed moves by a unit layer thickness creating a space for the printing of the next layer. Every single layer is stacked onto the previous layer. This goes on until the three-dimensional solid part is complete.[4–6] However, due to intrinsic process limitations, 3DP-FDM technology produced parts show lower mechanical strength and are anisotropic.[7–10] Bad surface finish and dimensional inaccuracies of 3D printed components are another matter of concern limiting its applications.[11] Furthermore, as 3D printing technology becomes more accessible, one important factor that still limits the creativity is the size of the printer or the printing volume. A 3D printer cannot print anything bigger than itself.[12] Most of the commercially available 3D printers come with a small build volume of 40–300 mm^3 making them less appropriate for 3D printing larger parts. Although big area additive manufacturing is an emerging technique in this field, which seems to address this issue, warpages and delamination during/after printing is again a matter to be looked upon.[13–15] A meaningful solution to the problem mentioned above could be welding of the 3D printed polymeric components resulting in a larger part.

Friction stir welding (FSW) is a relatively new, solid-state joining technique that was developed and patented by The Welding Institute (TWI) in 1991. At first, it was applied for welding of aluminum and its alloys, but later extended to magnesium, titanium alloys, welding of dissimilar metals and, more recently, even to polymeric materials.[16,17] Attempts have also been made to fabricate composites using this solid-state processing technique.[18] Among the various techniques available for welding of thermoplastics like hot gas welding, laser welding, ultrasonic welding, adhesive bonding; FSW has an upper hand in terms of non-emission of toxic gases as well as nonmelting of the base materials.[19,20] Small energy requirement, better quality of the weld joint, low process time, low machine/tool consumable costs, and environmental friendliness are the features, which are likely to make this technology a huge impact in industrial applications.[21–24] FSW technique makes use of a rotating tool having a shoulder and a profiled pin. The rotating tool is slowly plunged into the joint line of the parts to be welded. The substrates are clamped by a fixture and rigidly supported by a backing plate placed on the vertical machining center (VMC) bed. While traversing along the top surface of the substrates, the tool (shoulder and pin) remains in firm contact with a constantly applied load, generating the required frictional heat between the welding tool and the workpieces. This results in extreme stirring, reaching a state in which the softening of the material occurs. Subsequently, this leads to a solid-state adhesion between the two plates, resulting in a strong weld.[25,26] Figure 1 illustrates the FSW process showing the cross-sectional view of the tool, the designed fixture for clamping the plates that were used in the present research.

A literature review carried out revealed that the FSW of polymeric materials is currently one of the important areas of research. TWI has pioneered many innovative techniques and developed an extensive knowledge base and different processes for welding of plastics, leading to improved quality and greater productivity.[27] One of the earliest works on joining thermoplastics was demonstrated by Arici et al.,[28] wherein polyethylene plates were welded using the FSW technique. Mechanical performances of the FSW parts were explored and double passes were applied to eliminate the welding failures. Squeo et al.[29] investigated FSW of high-density polyethylene (HDPE), wherein the relationship between tool rotation speed, pin diameter, temperature, and feed rate on the weld quality was determined. The researchers found that these parameters considerably affected the properties of HDPE joints. Joining similar thermoplastics is relatively easier compared to the joining of dissimilar polymers because of the differences in thermo-mechanical properties between the two. FSW on dissimilar thermoplastics (polyethylene and polypropylene) was conducted by Eslami et al.[30] using a newly developed tool that resulted in the overall improvement of weld surface quality and strength. The researchers further concluded that the tensile strength of the specimen largely depended on the tool rotational and traversing speed. Singh et al.[31] in his work tried to join dissimilar plastics (ABS and PA6) with Al and Fe reinforcements. Tensile strength, hardness, and porosity percentages were determined for the welded components. Optimization of parameters like speed of rotation, process time, and rate of feed to execute welding was investigated and reported. Kumar et al.[32] explored the prospect of joining dissimilar 3D printed parts by equalizing their melt flow index (MFI) by the addition of Al nanoparticles. Al-reinforced ABS and PA6 thermoplastics were successfully joined by the FSW technique. The parts were further subjected to tensile, flexural, thermal, and micrographic analysis and it was reported that 15% Al with ABS and 50% Al with PA6 yielded maximum tensile and flexural strengths to the welded parts. As it could be observed that, although numerous research have been conducted on joining of similar, dissimilar, particle reinforced thermoplastics employing FSW technique, relatively lesser work could be seen on joining of 3D printed polymeric parts by FSW technique. Further, no work has been published so far to overcome the bed size limitation of a 3D printer by FSW technique. Besides, to the best of the knowledge of the authors, no research article could be found exploring the geometric

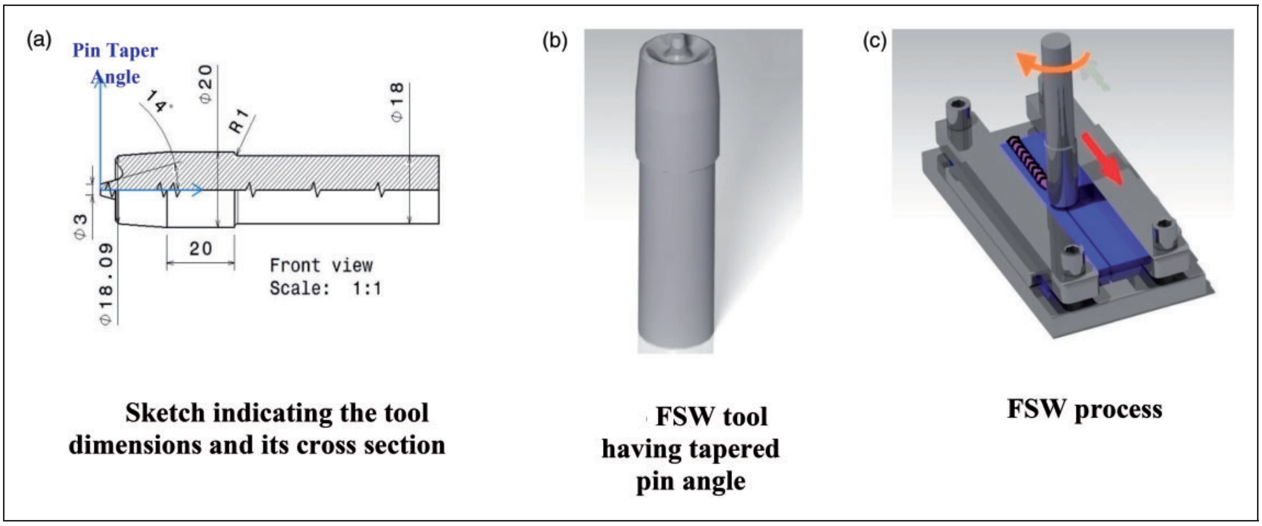

Figure 1. Schematic illustration of the FSW process: (a) sketch indicating the tool dimensions and its cross section; (b) FSW tool having tapered pin angle; (d) FSW process.

properties-flatness issues after welding of the two 3D printed parts.

In the present investigation, an attempt has been made to join similar/dissimilar 3D printed polymeric materials by the FSW technique. Optimization of various input parameters like parts infill percentages, material combination, tool rotational speed, traverse speed, and tool pin taper angle has been carried by means of design of experiments (DoE)–Taguchi L27–ANOVA technique. The effect of these parameters on the tensile strength, hardness as well as flatness of the FSW parts are explored and reported. This new scientific approach is expected to increase the capability of FSW while overcoming the limitations related to the bed size of a 3D printer.

Research methodology

Identification of important process parameters

The present investigation was carried out to weld similar/dissimilar polymeric materials using the FSW technique. In the process, important process parameters were identified and optimized using DoE. During the preliminary experiments on FSW, it was seen that between rotational speed of 900–1200 rev/min, traverse speed of 30–60 mm/min, and a tool pin taper angle of 10º–15º, the formation of the welds appeared to be defect-less. Hence, based on the pilot experiments and literature survey, following level of input variables were selected and optimized:

Tool rotational speed – Tool rotational speed plays a very important role during FSW of thermoplastics. An optimum tool rotation would result in sufficient material flow, creating a proper stirring action, generating a high amount of heat and finally a good weld. It has been recognized by several researchers that the weldability and strength of the weld largely depend on this parameter.[33,34] Therefore, to investigate and optimize the effect of this parameter on the strength of the parts welded, the same was considered.

Tool traverse speed – Tool traverse speed refers to the pace with which the friction stir welding tool advances along the weld line. Numerous researchers have reported the importance of tool traverse speed during the FSW process.[5,16,35] An optimum traverse speed controls the time duration of tool–workpeice interaction, controlling the heat input and finally affecting the crystallinity and resultant properties of the weld. It is also observed that this parameter affects the microstructure and the surface finish of the welded parts.[25] Hence, to assess the effect of this parameter on the mechanical and geometric properties of the joined parts, the same was considered.

Tool pin taper angle – Among the various tool geometries available (tool pin length, pin diameter, pin profile, pin taper angle, shoulder concavity angle, and shoulder diameter), tool pin taper angle plays a significant role determining the weld strength. Bicili et al.[36] and Vijay et al.[37] in their research varied the tool pin taper angle and discovered that larger pin taper angle results in larger fracture load, increasing the weld stir zone thicknesses producing a larger weld area. The researchers have further reported that a larger weld area produces larger weld tensile strengths. Hence, keeping these facts in view, this parameter was selected and optimized to analyze its effect on the strength and other properties of a 3D printed FSW part.

Infill – Infill is a very important parameter during 3D printing, which regulates the density of internal fillings of the polymeric parts.[38,39] The main objective of this study being joining of 3D printed polymers by the FSW technique, an end-user might not always go for 100% infill printing. Hence to evaluate the effect of different percentages of infill on the strength and

Table 1. Various process parameters with their levels.

		Levels		
Sl. no.	Process parameter	Level 1	Level 2	Level 3
1	Tool rotational speed (rev/min)	1000	1100	1200
2	Tool traverse Speed (mm/min)	30	40	50
3	Tool pin taper angle (°)	10	12	14
4	Infill (%)	80	90	100
5	Material combination	ABS + ABS	ABS + PETG	PETG + PETG

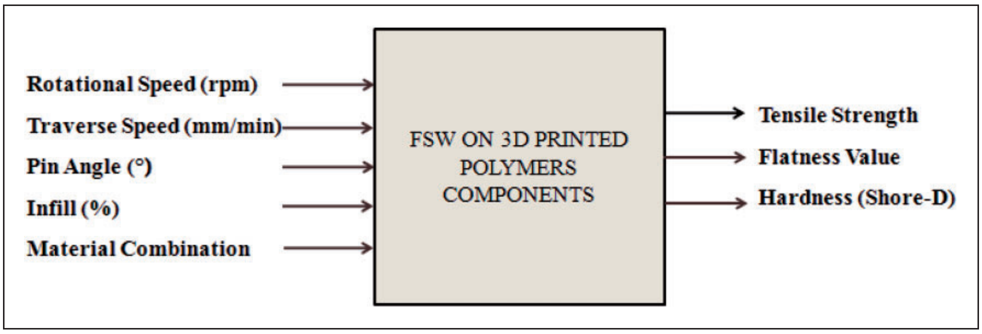

Figure 2. Input–output model of the DoE.
FSW: friction stir welding.

geometric tolerances of the FSW technique, the same was considered and optimized.

Material combination – The material combination on which FSW is carried out affects the joint's mechanical properties. While joining of similar thermoplastics is relatively easier, joining of dissimilar thermoplastics and attaining the desired level of properties is very difficult. This is due to the differences in their molecular weight, viscosity, melting point, MFI, and glass transition temperature (T_g).[31] Hence, to explore the possibility of joining dissimilar polymers by the FSW technique, three combinations of materials were selected and have been investigated.

Various process parameters considered along with their levels are given in Table 1.

Experimental design using design of experiments

The matrix of experiment having various input parameters and their levels was generated using the DoE–Taguchi technique using Minitab'16 software. A three-level, five-factor design having L27 runs was selected. A total of 27 experiments was conducted in the study. Further, process parameters were optimized by statistical analysis of variance (ANOVA) for obtaining the best output results. The input–output model for the various parameters investigated is as shown in Figure 2.

Fabrication of 3D printed parts

A 3D CAD model of $150 \times 40 \times 5\,mm^3$ (length × breadth × thickness) was created using CATIA V5. The file was exported with a .STL extension to the 3D printing machine's controller software – KISSlicer. The controller software converts this .STL file into G and M codes, regulating the pathway for the printing tool head to deposit the printing material. The 3D printing machine used in the present research work was Proto Centre 999, with an accessible printing volume of $240\,mm^3$, supplied by Aha Innovations Pvt. Ltd., Jaipur, India. Based on earlier work done by Kumar et al.,[32] it was realized that Melt

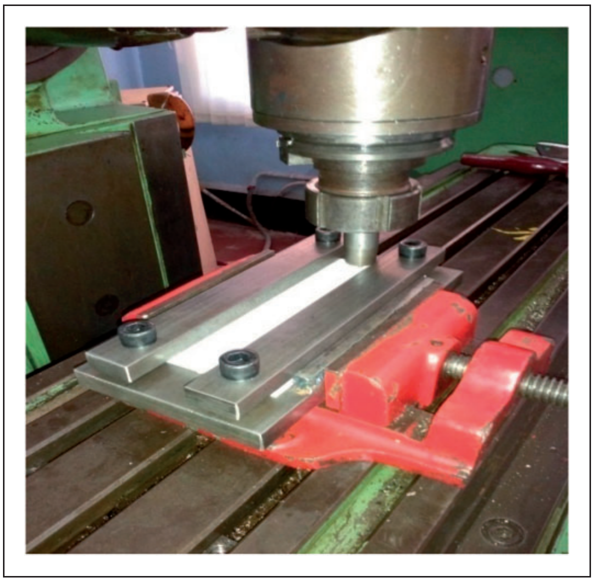

Figure 3. Experimental setup of the FSW process showing the designed fixture.

Table 2. DoE for input parameters and their levels, tensile strength, percentage elongation, flatness, and hardness numbers obtained after experimentation.

						Tensile test			Shore D hardness at different distances perpendicular to the weld section								
Sl. no.	Rotational speed (rev/min)	Traverse speed (mm/min)	Tool pin taper angle (°)	Infill (%)	Material combination	Strength (MPa)	Elongation at Break (%)	Flatness test (μ/m)	−12	−9	−6	−3	0	3	6	9	12
1	1000	30	10	80	ABS+ABS	13	6.5	0.064	77	76	65	60	57	64	68	71	73
2	1000	30	10	80	ABS+PETG	8.37	4.1	0.236	76	73	62	50	34	42	57	75	77
3	1000	30	10	80	PETG+PETG	12.5	13.7	0.201	76	75	68	60	55	60	70	78	78
4	1000	40	12	90	ABS+ABS	8.05	4.4	0.187	78	78	73	52	48	64	74	75	80
5	1000	40	12	90	ABS+PETG	10.5	13.9	0.138	77	76	78	63	58	65	73	78	79
6	1000	40	12	90	PETG+PETG	10.6	10.8	0.391	73	72	70	66	54	57	75	75	76
7	1000	50	14	100	ABS+ABS	19.3	7.8	0.119	78	77	75	73	66	70	74	76	76
8	1000	50	14	100	ABS+PETG	7.11	6.3	0.147	73	70	64	62	55	62	73	74	79
9	1000	50	14	100	PETG+PETG	16.6	17.2	0.09	73	73	68	65	54	68	69	68	72
10	1100	30	12	100	ABS+ABS	6.91	6.9	0.047	81	80	71	69	68	70	72	81	81
11	1100	30	12	100	ABS+PETG	14.3	13.2	0.156	76	71	68	63	54	57	68	73	74
12	1100	30	12	100	PETG+PETG	24.9	11.7	0.175	79	77	76	70	67	69	72	72	77
13	1100	40	14	80	ABS+ABS	25.7	8.4	0.192	75	74	73	71	69	72	75	76	79
14	1100	40	14	80	ABS+PETG	11.6	4.5	0.015	78	77	77	74	68	71	75	78	79
15	1100	40	14	80	PETG+PETG	31.9	32.7	0.193	77	77	65	62	60	68	75	78	79
16	1100	50	10	90	ABS+ABS	11.1	6.3	0.133	75	73	68	60	55	61	72	80	81
17	1100	50	10	90	ABS+PETG	5.62	8.5	0.177	73	72	62	55	46	72	74	74	74
18	1100	50	10	90	PETG+PETG	16.4	12.6	0.209	74	74	63	62	52	61	61	74	76
19	1200	30	14	90	ABS+ABS	18.5	9.2	0.047	77	74	74	70	63	78	78	79	79
20	1200	30	14	90	ABS+PETG	11.2	12.8	0.171	77	76	75	67	58	58	62	75	76
21	1200	30	14	90	PETG+PETG	11.2	10.8	0.076	79	78	68	62	52	64	66	79	80
22	1200	40	10	100	ABS+ABS	8.53	6.2	0.05	79	77	75	62	55	62	74	80	82
23	1200	40	10	100	ABS+PETG	13.3	6.9	0.146	80	78	63	57	53	66	68	74	74
24	1200	40	10	100	PETG+PETG	12.1	7.5	0.125	76	73	73	70	62	72	79	80	80
25	1200	50	12	80	ABS+ABS	15.2	5.6	0.09	79	76	68	67	60	65	72	78	79
26	1200	50	12	80	ABS+PETG	5.57	5.4	0.12	77	72	70	66	62	67	68	73	78
27	1200	50	12	80	PETG+PETG	7.79	8	0.162	81	78	78	74	59	65	76	80	80

Flow compatibility between the two polymers is an important aspect to be looked upon while selecting the two polymers. Virgin ABS shows an MFI of 9.05 g/10 min, while virgin PETG shows a value of 8 g/10 min measured as per ASTM D1238. The difference in the MFI between the two polymers being very less, ABS and PETG were selected for the present study. The total number of parts printed was 54 in number, while 27 trials of experiments were conducted as per the DoE.

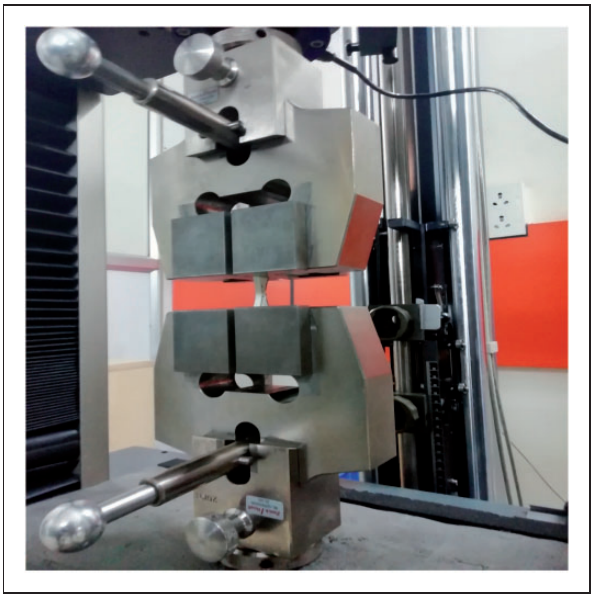

Figure 4. Tensile testing on the welded joints.

Friction stir welding of 3D printed parts

FSW of 3D printed polymeric parts was carried out on a three-axis VMC. The parts to be welded were 3D printed with two polymeric materials, i.e. ABS and PETG with various infill percentages. During the process of FSW, various combinations of the two $150 \times 40 \times 5\,mm^3$ polymeric plates were butted tightly together. The joint line was secured using a clamping fixture as shown in Figure 3. The tool employed in the research was made of mild steel material with a hardness of 53 HRC. Different pin taper angled rotating tools were employed for the process. The rotating tool was set at different levels of speeds and then plunged into the butted parts at one end. A dwell time of 10 s was allowed resulting in the formation of a small pool of plasticized material after which the tool traversed along the butt line forming a joint. After welding, the

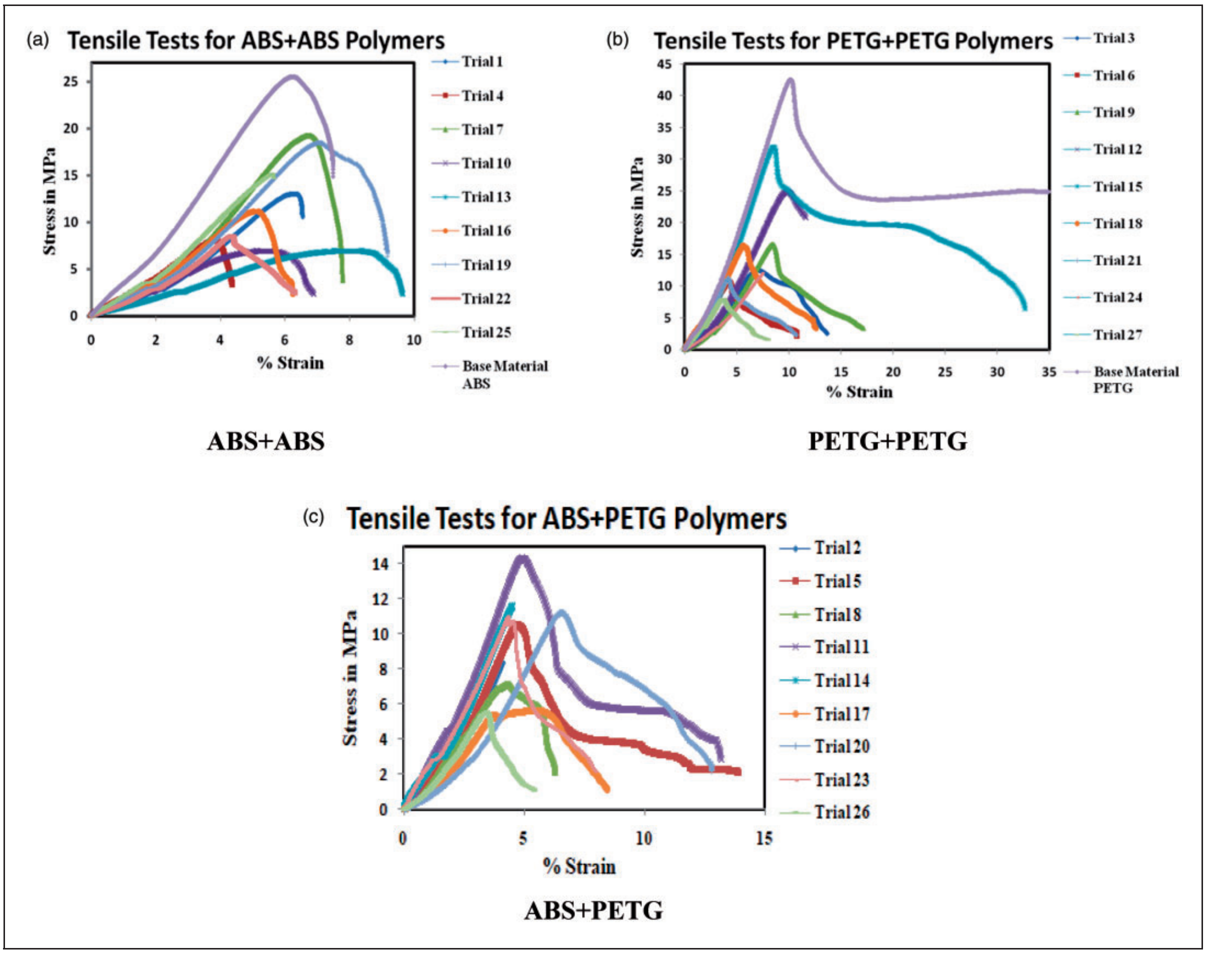

Figure 5. Tensile stress–strain curves for different polymer combinations: (a) ABS + ABS; (b) PETG + PETG; (c) ABS + PETG.

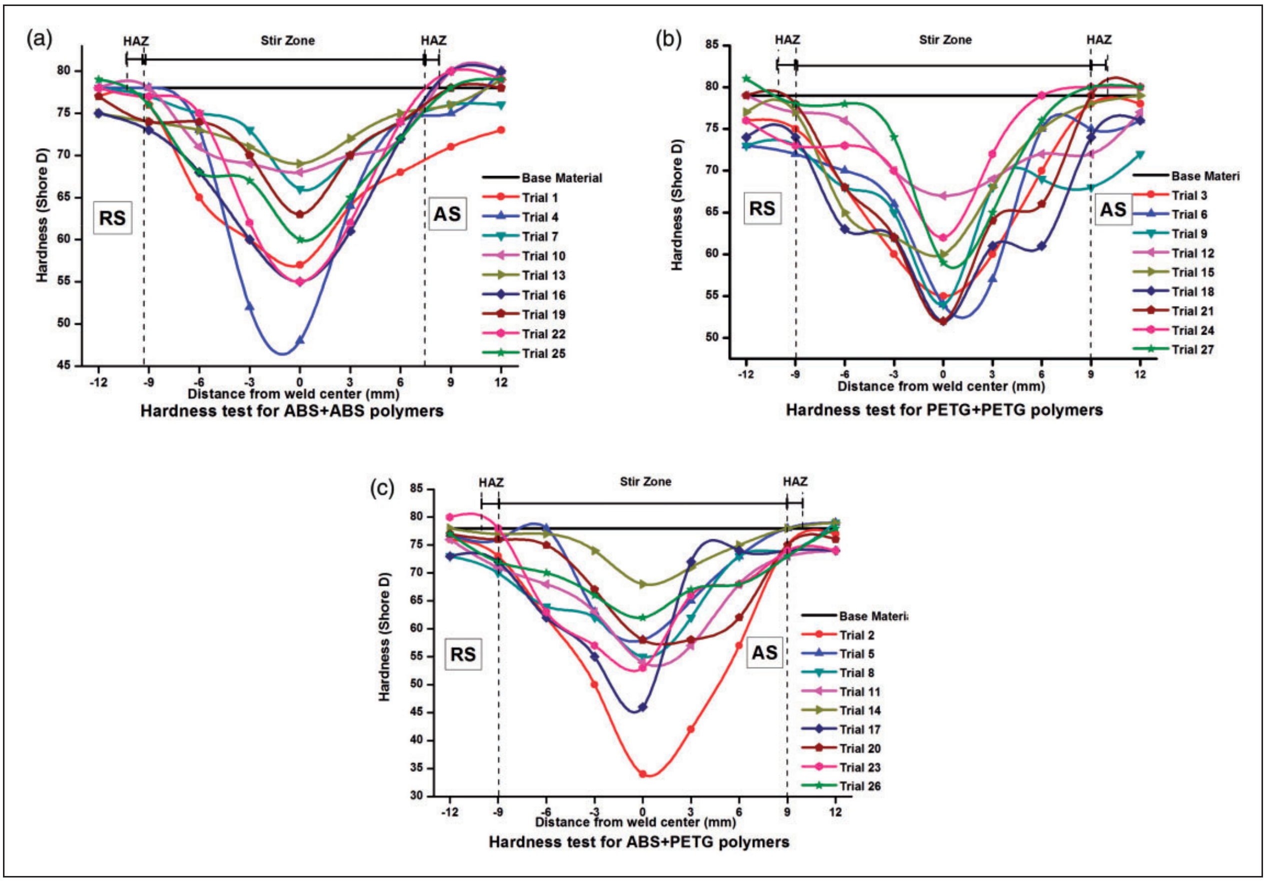

Figure 6. Hardness profiles of the welded joints fabricated by FSW technique on various 3D printed parts.
HAZ: heat-affected zone; AS: advancing side; RS: retreating side.

welds were allowed to cool in the fixture for about 5 min preventing any warpages in the weld zone. The trials were conducted as per the DoE Table 2. Only single pass FSW was carried out and the welded parts were taken for further testing and properties evaluation.

Results and discussion

Effect of process parameters on the tensile strength of welded parts

Tensile test samples were extracted from each welded joint and tests were conducted as per the ASTM D-638 type V standard, on a universal testing machine (Zwick Roell, Z020, load cell 20Z kN), at a crosshead speed of 3 mm/min. The tensile testing setup is shown in Figure 4. The test specimens were cut perpendicular to the weld line using an electrical zig-zag cutting machine. Three test specimens were taken from each of the welds and tested for their mechanical strength and percentage elongation at break. The average results of the tensile test of the joints with various material combinations are shown in Figure 5, while the results obtained are presented in the DoE Table 2.

From the graphs, it can be inferred that the welded joints fractured in a ductile mode showing some percentage elongation after attaining the ultimate tensile strength. The strengths of the welded joints, for all combinations, came out to be lesser than their base material (ABS – 25 MPa, PETG – 43 MPa). The decrement in the tensile strength is largely attributed to the presence of wormhole and lack of penetration (LOP) defect. These defects resulted in discontinuities along the weld line resulting in poor tensile strength. Additionally, thermoplastics have low thermal conductivity (lower than $0.5\,W{\cdot}m^{-1}{\cdot}K^{-1}$), stirring might not have happened properly leading to the improper material flow. This might have also resulted in the weld defects, subsequently decreasing the weld strength. The decrement in the tensile strength due to defects has been also reported by Simões et al.[40] and Azhiri et al.[41] Further, intermittent fine voids were also noticed in the weld region. This is believed to be because of the following reasons: firstly, the pre-existing empty spaces in the 3D printed plates fabricated with various infills, particularly observed for 80% and 90% can be a reason for this. Secondly, the staircase effect (due to layer-by-layer deposition), usually seen at the edges of 3D printed parts might have caused the voids after the FSW. Besides, the present welds were made from single-pass, which was not sufficient to annihilate this problem. The above observations imply that FSW of 3D printed parts (for both similar/dissimilar) produced weaker joints compared to the base material. Based on

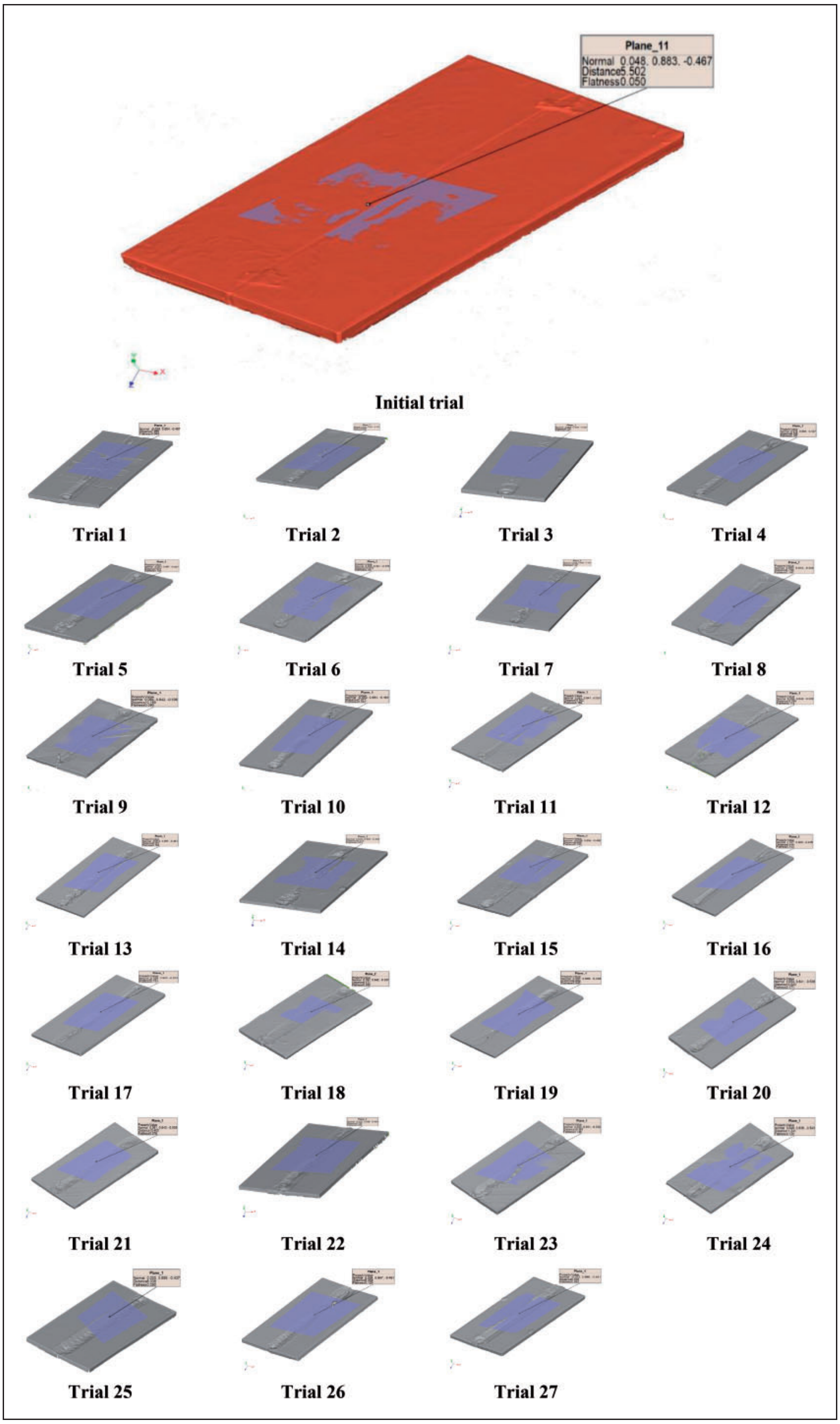

Figure 7. Flatness values of the welded joints fabricated by FSW technique on various 3D printed parts.

Table 2, the maximum tensile properties (31.9 MPa and 32.7% elongation) were observed for the material combination PETG+PETG (Trial 15), with the input parameter set as 1100 rev/min, 40 mm/min, 14°, and 80% infill.

Effect of process parameters on the hardness of the welded parts

The study of the hardness on the FSW parts is important in knowing the mechanical strength of the joints.[42]

Table 3. Variation of SN ratios over input process variables.

Expt. no.	SN (tensile strength (MPa))	SN (percentage elongation (%))	SN (flatness (μ/m))
1	22.2789	16.2583	23.8764
2	18.4545	12.2557	12.5418
3	21.9382	22.7344	13.9361
4	18.1159	12.8691	14.5632
5	20.4238	22.8603	17.2024
6	20.5061	20.6685	8.1565
7	25.7111	17.8419	18.4891
8	17.0374	15.9868	16.6537
9	24.4022	24.7106	20.9151
10	16.7896	16.7770	26.5580
11	23.1067	22.4115	16.1375
12	27.9240	21.3637	15.1392
13	28.1987	18.4856	14.3340
14	21.2892	13.0643	36.4782
15	30.0758	30.2910	14.2889
16	20.9065	15.9868	17.5230
17	14.9947	18.5884	15.0405
18	24.2969	22.0074	13.5971
19	25.3434	19.2758	26.5580
20	20.9844	22.1442	15.3401
21	20.9844	20.6685	22.3837
22	18.6190	15.8478	26.0206
23	22.4770	16.7770	16.7129
24	21.6557	17.5012	18.0618
25	23.6369	14.9638	20.9151
26	14.9171	14.6479	18.4164
27	17.8307	18.0618	15.8097

SN: signal-to-noise.

In our study, shore D hardness was measured using a Durometer (Yuzuki make) instrument. The tests were carried as per the ASTM D2240 standard. Figure 6 shows the hardness distribution along the perpendicular direction (-12 to $+12$ mm) to the welded joint line for different trials. Considering the plunging of the tool shoulder done during the trials, the stir zone was taken throughout -9 to $+9$ mm from the center of the weld. There was no obvious heat-affected zone (HAZ) due to the low thermal conductivity of the thermoplastics. Flash of the polymers was consistently present along the weld edge on the left hand side helping us identify the retreating side (RS). The weld zone showed a lower hardness value compared to their base material. This drop in the hardness value is reasoned to be because of the change in the mechanical properties due to the change of molecular weight/crystallinity caused by the high cooling rate.[22] Figure 6(a) shows the hardness value slightly higher that the base material in the HAZ on the advancing side (AS). This could be because of some amount of localized heating as well as uneven distribution of crystallinity. The highest hardness value was observed for the material combination of ABS+ABS (69 Shore D, for Trial 13) with the input parameter set as 1100 rev/min, 40mm/min, 14°, and 80% infill.

Flatness tests on the FSW parts

The quality of a weld depends upon the flatness of the plate surface produced after the welding operation. Many of the industrial applications ask for a high degree of flatness for their requirements. In our research, the welded components were scanned using a "Zeiss 3D scanner" with 30 μm quoted accuracy. Further, the flatness values were determined using Inspect^{+} Software. The flatness values measured are as shown in Figure 7. The flatness value for the base material, without FSW being done was around 0.05 μ/m. Further, on comparing the various flatness values (Table 2), we could observe that it varied from 0.015 to 0.391 μ/m. Lower the flatness value, more flat would be the welded joint. It could be observed that the highest flatness was observed for the material combination of ABS+PETG (0.015 μ/m, for trial 14), with the input parameter set as 1100 rev/min, 40 mm/min, 14º, and 80% infill. The flatness readings obtained were for two 150 mm plates welded by FSW. However, this value would change for different lengths of the workpieces taken. The standard deviation seen in the flatness value was 0.075 μ/m, which means that there was better control over the flatness. Further, it could also be seen that the heat-affected zone didn't affect the level of flatness. This proves that the process is a feasible technique for industrial requirements/applications where a high degree of flatness is expected after joining.

Optimization of the process parameters

The trials were conducted as per the generated DoE table. The input and output parameters considered are as discussed in Figure 2. The various levels of input parameters considered during the experiments are as discussed in Table 1. The results obtained after carrying out the trials are as shown below (Table 2).

For optimizing the input parameters and selecting the best contributing process parameters, signal-to-noise ratio (SN) was determined. The SN ratio is always expected to be the maximum, with material properties transfer to SN ratio as "larger the better" or "smaller the better". For the mechanical properties: tensile strength and percentage elongation, larger the better was selected, with the SN ratio was calculated using

$$\eta = -10 \log\left[\frac{1}{\mathrm{n}}\sum_{k=1}^{n}\frac{1}{\mathrm{y}^2}\right] \tag{1}$$

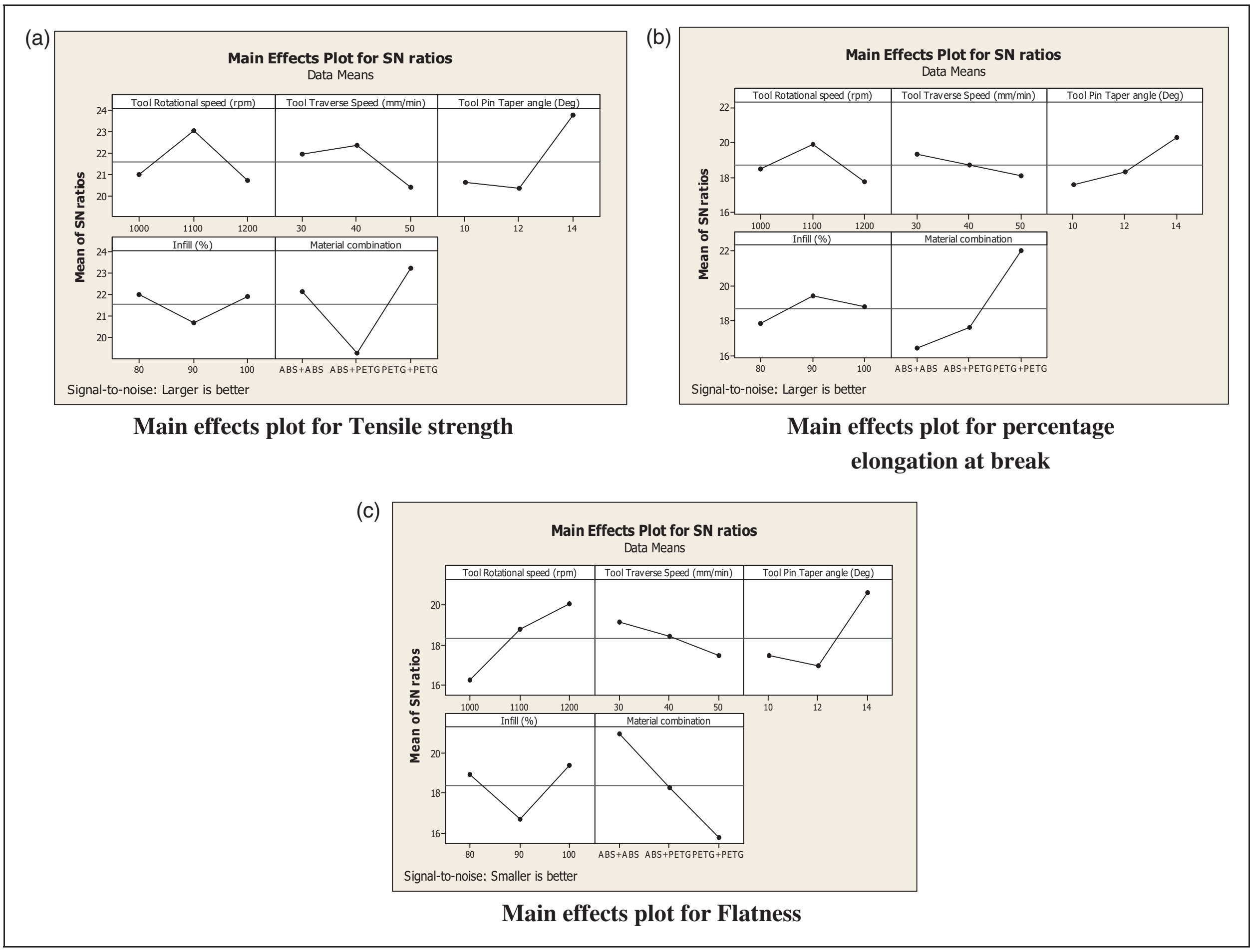

Figure 8. Graphs showing the main effects of various input parameters: (a) main effects plot for tensile strength; (b) main effects plot for percentage elongation at break; (c) main effects plot for flatness.
SN: signal-to-noise.

Table 4. ANOVA analysis for strength.

Source	Degrees of freedom	Sum of squares	Adjacent sum of squares	Adjacent mean of squares	Fisher's value	Probability	Percentage contribution
Tool rotational speed (rev/min)	2	29.73	29.73	14.86	1.25	0.312	7.613
Tool traverse speed (mm/min)	2	19.31	19.31	9.65	0.81	0.461	4.94
Tool pin taper angle (°)	2	65.17	65.17	32.59	2.75	0.094	16.69
Infill (%)	2	10.04	10.04	5.02	0.42	0.662	2.57
Material combination	2	76.40	76.40	38.20	3.22	0.067	19.56
Error	16	189.82	189.82	11.86			48.61
Total	26	390.47					

Table 5. Response table for signal-to-noise ratios for strength.

Level	Tool rotational speed (rev/min)	Tool traverse speed (mm/min)	Tool pin taper angle (°)	Infill (%)	Material combination
1	20.99	21.98	20.62	22.07	22.18
2	23.06	22.37	20.36	20.73	19.30
3	20.72	20.41	23.78	21.97	23.29
Delta	2.35	1.96	3.42	1.34	3.99
Rank	3	4	2	5	1

Table 6. Predicted versus actual value of output parameter at the optimal predicted setting.

Properties	Strength (MPa)	Elongation (%)	Flatness (μ/m)
Predicted value	25.7473	20.20	0.048
Actual value	31.2	14.7	0.047

For properties like flatness, smaller the better was selected, with the SN ratio calculated using

$$\eta = -10\log\left[\frac{1}{\mathrm{n}}\sum_{k=1}^{n}\mathrm{y}^2\right] \tag{2}$$

where η is the SN ratio, n is the number of experiment, and y is the material properties at experiment number k. The variation of SN ratios for input variables is shown in the Table 3 (based on the DoE in Table 2).

From Table 3, the main effect plots (Figure 8) were plotted to see the effect of tool rotational speed, tool traverse speed, tool pin taper angle, infill percentage, and material combinations on mechanical properties and flatness of the 3D printed FSW parts.

Further, analysis of variance (ANOVA) table was developed to evaluate the effect of process parameters on specific properties, relating the SN ratios with the input parameters. Table 4 shows the ANOVA analysis for strength as an example of computation. As observed, the material combination (percentage contribution and probability value), proved to be significant.

On the basis of Table 4, Table 5 is formed showing the ranking of the input process parameters.

Using the following equation, the best possible value of strength for this case can be predicted

$$\mathrm{n_{opt}} = \mathrm{m} + (\mathrm{m_{A2}} - \mathrm{m}) + (\mathrm{m_{B2}} - \mathrm{m}) + (\mathrm{m_{C3}} - \mathrm{m}) + (\mathrm{m_{D1}} - \mathrm{m}) + (\mathrm{m_{E3}} - \mathrm{m}) \tag{3}$$

where "m" is the overall mean of SN ratio, $\mathrm{m_{A2}}$ is the mean of SN ratio for rotational speed at level 2, $\mathrm{m_{B2}}$ is the mean of SN ratio for transverse speed at level 2, $\mathrm{m_{C2}}$ is the mean of SN ratio for tool pin angle, $\mathrm{m_{D1}}$ is the mean of SN ratio for infill%, and $\mathrm{m_{D3}}$ is the mean of SN ratio for material combination.
The overall mean of SN ratio (m) was taken from Minitab software

$\mathtt{m} = 21.5884$ db (from Table 4)
$\mathtt{m_{A2}} = 23.06$, $\mathtt{m_{B2}} = 22.37$, $\mathtt{m_{C3}} = 23.78$, $\mathtt{m_{D1}} = 22.07$, $\mathtt{m_{E3}} = 23.29$
$\mathtt{n_{opt}} = 21.58884 + (23.06\text{-}21.58884) + (22.37\text{-}21.58884) + (23.78\text{-}21.58884) + (22.07\text{-}21.58884) + (23.29\text{-}21.58884)$
$\mathtt{n_{opt}} = 28.21464$

$$\mathtt{y^2_{opt}} = (10)^{\frac{\mathrm{n_{opt}}}{10}} \tag{4}$$

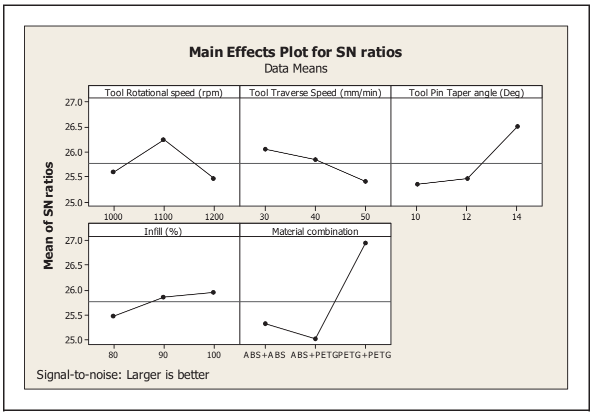

Figure 9. Graphs showing the combined optimized set of process parameters.

$\mathtt{y^2_{opt}} = 662.924$
$\mathtt{y_{opt}} = 25.7473$

The predicted optimum value for strength = 25.7473 MPa.

In the same manner, the process parameter as well as the optimum value can be predicted for percentage elongation as well. For predicting the optimum value for flatness, equation (4) should be replaced by equation (5)

$$\mathrm{y^2_{opt}} = \left(\frac{1}{10}\right)^{\frac{\mathrm{n_{opt}}}{10}} \tag{5}$$

From Tables 3, 4, and 5, the predicted and experimentally determined values of output parameters (tensile strength, percentage elongation, and flatness) have been shown in Table 6.

Combined optimization of the process parameters

For determining combined optimization of the process parameters, the SN ratios of all the properties were combined by selecting SN ratios on larger the better basis. Tool rotation speed of 1100 rev/min, transverse speed of 30 mm/min, pin angle, of 14° 100% infill, and PETG+PETG resulted as the best set of input process parameters (see Figure 9).

Since the probability value of material combination was obtained as 0.016 (lower than 0.05), the combined optimized setup is predicted as significant. The material combination appeared as most contributing factors

Table 7. ANOVA analysis for SN ratios.

Source	Degrees of freedom	Sum of squares	Adjacent sum of squares	Adjacent mean of squares	Fisher's value	Probability	Percentage contribution
Tool rotational speed (rev/min)	2	3.189	3.189	1.595	0.89	0.431	5.152
Tool traverse speed (mm/min)	2	1.975	1.975	0.988	0.55	0.588	3.19
Tool pin taper angle (°)	2	7.366	7.366	3.638	2.05	0.162	11.9
Infill (%)	2	1.123	1.123	0.562	0.31	0.736	1.81
Material combination	2	19.459	19.459	9.730	5.41	0.016	31.43
Error	16	28.785	28.785	1.799			46.50
Total	26	61.897					

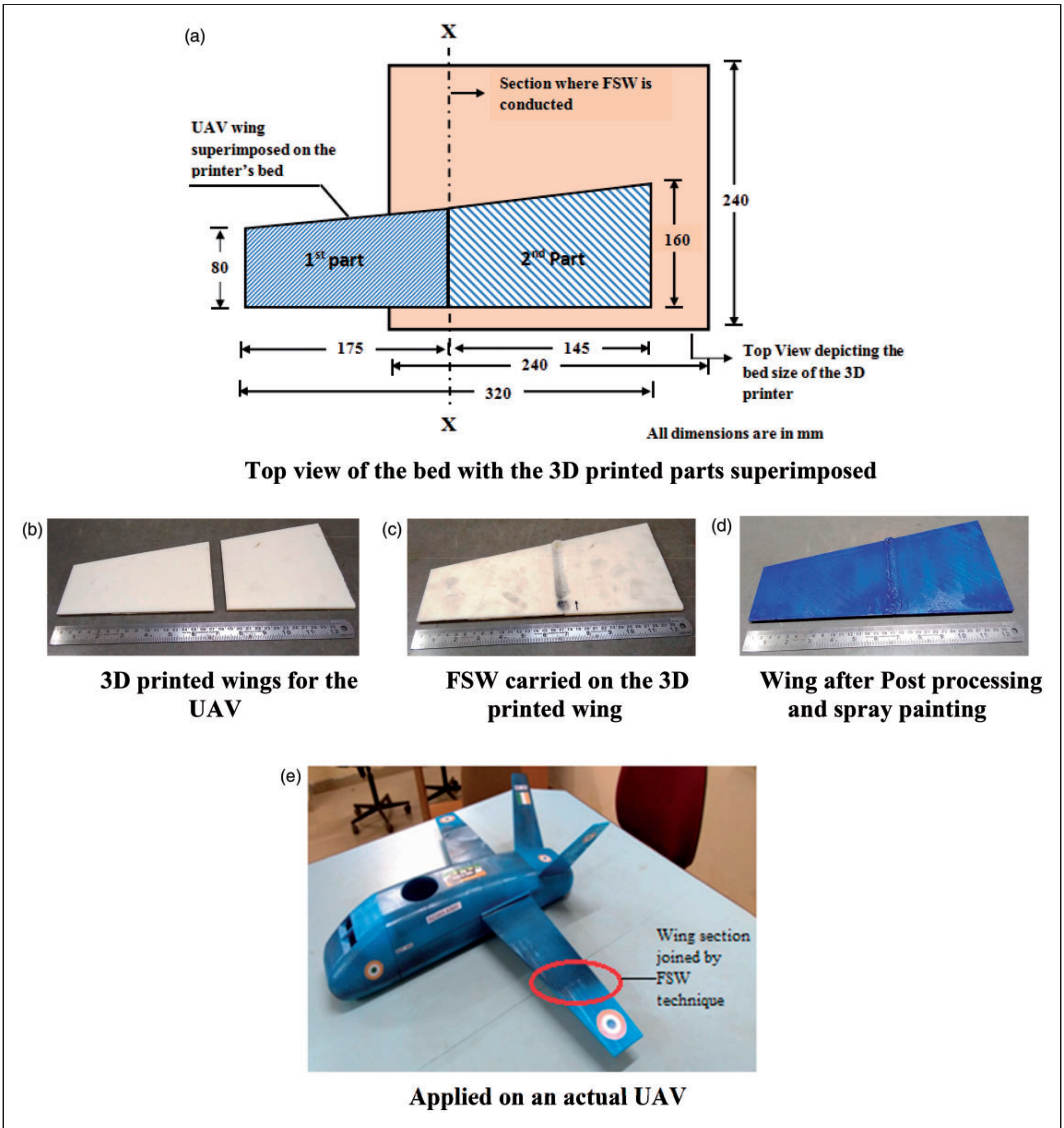

Figure 10. Application of the proposed technique on an UAV: (a) top view of the bed with the 3D printed parts superimposed; (b) 3D printed wings for the UAV; (c) FSW carried on the 3D printed wing; (d) wing after post processing and spray painting; (e) applied on an actual UAV.
UAV: unmanned aerial vehicle; FSW: friction stir welding.

with 31.43% contributing percentage. Tool pin taper angle was the next important contributing factor with an 11.9% contribution (see Table 7). Optimization of the process parameters (earlier two sections) was carried out by referring to the works done previously.[31,43–47]

Application of FSW of 3D printed parts on an unmanned aerial vehicle

The experimental work carried out in the previous sections was applied to join segment of a 3D printed UAV wing. The process parameters while carrying out the 3D printing as well as the FSW process was based on the results obtained from the combined optimization (previous section). The process parameters were set as PETG+PETG material combination, 100% infill, 1100 rev/min tool rotation speed, 30 mm/min traverse speed, and 14° tool taper pin angle. The maximum bed size of the available 3D printer was 240 mm, while the actual requirement was 320 mm (x-direction). Figure 10(a) shows the UAV wing superimposed on the 3D printer bed platform. Figure 10(b) shows the two 3D printed wing sections (175 and 145 mm length) printed after cutting the CAD model using the NETFABB software. Figure 10(c) shows the two wing sections joined by the FSW technique. Flatness test conducted on the joined component showed a value of 0.41 μ/m, which is acceptable as per the industrial standards. This validated the usefulness of the proposed technique providing flexibility in fabricating 3D printed parts with higher aspect ratios. Later, post processing was carried out to improve the aesthetics for the final application. Figure 10(d) shows the post processed joint component after spray painting, while Figure 10(e) shows the final assembled 3D printed UAV with the FSW wing.

Conclusion

The investigation was carried out to join 3D printed similar/dissimilar thermoplastics by the FSW technique. Few critical parameters related to 3D printing as well as FSW, namely infill percentage, material combination, tool rotational speed, traverse speed, and tool pin taper angle were optimized using the statistical tool, ANOVA. These parameters were optimized to obtain the best tensile strength, elongation, hardness as well as higher flatness level. Finally, the optimized set of parameters were applied to join the wing section of a UAV. The following conclusions are drawn from the investigation:

- The tensile strengths of the welded joints for all combinations were found to be relatively lesser than their base material (ABS–25 MPa, PETG–43 MPa). Future studies can be aimed at improving the tensile strength of the joint by using metal/polymer grafted 3D printed components.
- The hardness at the welded joint was less than the hardness of the base materials due to low crystallinity resulting from high cooling rate of thermoplastics.
- Standard deviation in flatness was observed to be 0.075 μ/m, which indicated that there was better control over the flatness level.
- Studies from statistical analysis (ANOVA) implied that the type of material combination and tool pin taper angle play a significant role in the weld's strength as well as its geometric properties.
- The optimized parameters were used to fabricate a wing of a UAV with a span of 320 mm using a 3D printer having a maximum permissible size of 240 mm. The joint quality was enhanced with an acceptable flatness value of 0.41 μ/m. Therefore, the proposed method provides leeway in fabricating 3D printed parts possessing higher aspect ratios.

Acknowledgements

The authors are thankful to Visveswaraya Technological University (VTU), Jnana Sangama, Belagavi for the research encouragements. They also thank Mr Abduljabbar B Khan – Department of Mechanical Engineering for CAD modeling the tool, fixture and Dr Nikhil R – Department of Mechanical Engineering for scanning the components for flatness evaluation.

Declaration of Conflicting Interests

The author(s) declared no potential conflicts of interest with respect to the research, authorship, and/or publication of this article.

Funding

The author(s) disclosed receipt of the following financial support for the research, authorship, and/or publication of this article: The research work was funded by the Government of Karnataka (GOK) under Karnataka Council for Technological Upgradation (KCTU) research grant and KLSGIT, Belagavi. The research facilities were provided in "Additive and Reverse Engineering Lab" by KLSGIT, Belagavi.

ORCID iD

Vinayak Malik https://orcid.org/ 0000-0002-9863-5738

Supplemental material

Supplemental material for this article is available online.

References

1. Zhu J, Hu Y, Tang Y, et al. Effects of styrene–acrylonitrile contents on the properties of ABS/SAN blends for fused deposition modelling. *J Appl Polym Sci* 2016; 133.
2. Gnanasekaran K, Heijmansa T, van Bennekom S, et al. 3D printing of CNT- and graphene-based conductive

polymer nanocomposites by fused deposition modelling. *Appl Mater Today* 2017; 9: 21–28.
3. Aslanzadeh S, Saghlatoon H, Honari MM, et al. Investigation on electrical and mechanical properties of 3D printed nylon 6 for RF/microwave electronics applications. *Addit Manuf* 2018; 21: 69–75.
4. Tao Y, Wang H, Li Z, et al. Development and application of wood flour-filled polylactic acid composite filament for 3D printing. *Materials* 2017; 10: 334.
5. Jia Y, He H, Geng Y, et al. High through-plane thermal conductivity of polymer based product with vertical alignment of graphite flakes achieved via 3D printing. *Compos Sci Technol* 2017; 145: 55–61.
6. Osswald TA, Puentes J and Kattinger J. Fused filament fabrication melting model. *Addit Manuf* 2018; 22: 51–59.
7. Perez ART, Roberson DA and Wicker RB. Fracture surface analysis of 3D-printed tensile specimens of novel ABS-based materials. *J Fail Anal Prev* 2014; 14: 343–353.
8. Torrado AR, Shemelya CM, English JD, et al. Characterizing the effect of additives to ABS on the mechanical property anisotropy of specimens fabricated by material extrusion 3D printing. *Addit Manuf* 2015; 6: 16–29.
9. Weng Z, Wang J, Senthil T, et al. Mechanical and thermal properties of ABS/montmorillonite nanocomposites for fused deposition modeling 3D printing. *Mater Des* 2016; 102: 276–283.
10. Zaldivar RJ, Witkin DB, McLouth TD, et al. Influence of processing and orientation print effects on the mechanical and thermal behaviour of 3D-printed ULTEM® 9085 material. *Addit Manuf* 2017; 13: 71–80.
11. Tiwary V, Arunkumar P, Deshpande A, et al. Studying the effect of chemical treatment and fused deposition modelling process parameters on surface roughness to make acrylonitrile butadiene styrene patterns for investment casting process. *Int J Rapid Manuf* 2015; 5: 276–288.
12. How to 3D-print objects larger than your 3D printer, http://mashable.com/2013/09/19/3d-print-large-objects/#qvvPEe2aBqqg (accessed 23 May 2019).
13. Barnett E and Gosselin C. Large-scale 3D printing with a cable-suspended robot. *Addit Manuf* 2015; 7: 27–44.
14. Kishore V, Ajinjeru C, Nycz A, et al. Infrared preheating to improve interlayer strength of big area additive manufacturing (BAAM) components. *Addit Manuf* 2017; 14: 7–12.
15. Cincinnati incorporated big area additive manufacturing, https://www.e-ci.com/baam/ (accessed 20 June 2019).
16. Bandari V and Sharma A. Induction heated tool assisted friction-stir welding (i-FSW): a novel hybrid process for joining of thermoplastics. *J Manuf Process* 2015; 20: 234–244.
17. Kiss Z and Czigány T. Microscopic analysis of the morphology of seams in friction stir welded polypropylene. *Express Polym Lett* 2012; 6: 54–62.
18. Bajakke PA, Malik VR and Deshpande AS. Particulate metal matrix composites and their fabrication via friction stir processing – a review. *Mater Manuf Process* 2018; 34: 833–881.
19. Azhiri RB, Tekiyeh RM, Zeynali E, et al. Measurement and evaluation of joint properties in friction stir welding of ABS sheets reinforced by nanosilica addition. *Measurement* 2018; 127: 198–2014.
20. Spaggiari A and Denti F. Mechanical Strength of adhesively bonded joints using polymeric additive manufacturing. *Proc IMechE, Part C: J Mechanical Engineering Science* 2019.
21. Quintana KJ and Silveira JL. Mechanistic models and experimental analysis for the torque in FSW considering the tool geometry and the process velocities. *J Manuf Process* 2017; 30: 406–417.
22. Huang Y, Meng X, Xie Y, et al. Friction stir welding/processing of polymers and polymer matrix composites. *Compos Part A: Appl Sci Manuf* 2018; 105: 235–257.
23. Eslami S, Ramos T, Paulo J, et al. Effect of friction stir welding parameters with newly developed tool for lap joint of dissimilar polymers. *Procedia Eng* 2015; 114: 99–207.
24. Malik VR and Kailas SV. Plasticine modeling of material mixing in friction stir welding. *J Mater Process Technol* 2018; 258: 80–88.
25. Givi MKB and Asadi P. *Advances in friction stir welding and processing*. Cambridge: Woodhead Publishers, 1981.
26. Lambiase F, Paoletti A and Ilio AD. Forces and temperature variation during friction stir welding of aluminum alloy AA6082-T6. *Int J Adv Manuf Technol* 2019; 99: 337–346.
27. www.twi-global.com/what-we-do/research-and-technology/technologies/welding-joining-and-cutting/polymer-welding, The Welding Institute, Polymer Welding (accessed 19 June 2019).
28. Arici A and Sinmaz T. Effect of double passes of the tool on friction stir welding of polyethylene. *J Mater Sci* 2015; 40: 3313–3316.
29. Squeo EA and Bruno G. Friction stir welding of polyethylene sheets. In: *The annals of "Dunarea De Jos", University of Galati Fascicle V*. Technologies in Machine Building, 2009.
30. Eslami S, Ramos T, Tavares PJ, et al. Shoulder design developments for FSW lap joints of dissimilar polymers. *J Manuf Process* 2015; 20: 15–23.
31. Singh R, Kumar R, Feo L, et al. Friction welding of dissimilar plastic/polymer materials with metal powder reinforcement for engineering applications. *Compos Part B: Eng* 2016; 101: 77–86.
32. Kumar R, Singh R and Ahuja IPS. Mechanical, thermal and micrographic investigations of friction stir welded: 3D printed melt flow compatible dissimilar thermoplastics. *J Manuf Process* 2019; 38: 387–395.
33. Elyasi M and Derazkola HA. Experimental and thermomechanical study on FSW of PMMA polymer T-joint. *Int J Adv Manuf Technol* 2018; 97: 1445–1456.
34. Azdast T, Hasanzadeh R and Moradian M. Improving impact strength in FSW of polymeric nanocomposites using stepwise tool design. *Mater Manuf Process* 2018; 33: 343–349.
35. Padhy GK, Wu CS and Gao S. Friction stir based welding and processing technologies - processes, parameters, microstructures and applications: a review. *J Mater Sci Technol* 2018; 34: 1–38.
36. Bilici MK. Effect of tool geometry on friction stir spot welding of polypropylene sheets. *eXPRESS Polym Lett* 2012; 6: 805–813.

37. Vijay SJ and Murugan N. Influence of tool pin profile on the metallurgical and mechanical properties of friction stir welded Al–10 wt. % TiB2 metal matrix composite. *Mater Des* 2010; 31: 3585–3589.
38. Tiwary VK, Arunkumar P, Deshpande AS, et al. Surface enhancement of FDM patterns to be used in rapid investment casting for making medical implants. *Rapid Prototyp J* 2019; 25: 904–914.
39. Kerekes TW, Lim H, Joe WY, et al. Characterization of process–deformation/damage property relationship of fused deposition modeling (FDM) 3D-printed specimens. *Addit Manuf* 2019; 25: 532–544.
40. Simões F and Rodrigues DM. Material flow and thermo-mechanical conditions during Friction Stir Welding of polymers: literature review, experimental results and empirical analysis. *Mater Des* 2013.
41. Bagherian Azhiri R, Mehdizad Tekiyeh R, Zeynali E, et al. Measurement and evaluation of joint properties in friction stir welding of ABS sheets reinforced by nanosilica addition. *Measurement* 2018.
42. Derazkola HA and Elyasi M. The influence of process parameters in friction stir welding of Al-Mg alloy and polycarbonate. *J Manuf Process* 2018; 35: 88–98.
43. Kumar R, Singh R and Ahuja I. Friction stir welding of ABS-15Al sheets by introducing compatible semiconsumable shoulder-less pin of PA6-50Al. *Measurement* 2018.
44. Kumar R, Singh R and Ahuja IPS. Friction stir welding of 3D printed melt flow compatible dissimilar thermoplastic composites. *Proc IMechE, Part C: J Mechanical Engineering Science* 2019.
45. Singh R, Kumar R and Ahuja IPS. Mechanical, thermal and melt flow of aluminum-reinforced PA6/ABS blend feedstock filament for fused deposition modelling. *Rapid Prototyp J* 2018.
46. Kumar R, Singh R, Ahuja IPS, et al. Friction welding for the manufacturing of PA6 and ABS structures reinforced with Fe particles. *Compos Part B: Eng* 2017.
47. Ahmadi H, Mostafa Arab NB and Ashenai Ghasemi F. Optimization of process parameters for friction stir lap welding of carbon fibre reinforced thermoplastic composites by Taguchi method. *J Mech Sci Technol* 2014.